Tunable spin-orbit-coupled Bose-Einstein condensates in deep optical lattices

M. Salerno,[1] F. Kh. Abdullaev,[2,3] A. Gammal,[4] and Lauro Tomio[2,5,6]

[1]*Dipartimento di Fisica "E.R. Caianiello," CNISM and Istituto Nazionale di Fisica Nucleare—Gruppo Collegato di Salerno, Universitá di Salerno, Via Giovanni Paolo II, 84084 Fisciano (SA), Italy*

[2]*Centro de Ciências Naturais e Humanas, Universidade Federal do ABC, 09210-170 Santo André, Brazil*

[3]*Department of Physics, Kulliyyah of Science, International Islamic University Malaysia, 25200 Kuantan, Malaysia*

[4]*Instituto de Física, Universidade de São Paulo, 05508-090 São Paulo, Brazil*

[5]*Instituto Tecnológico de Aeroáutica, CTA, 12228-900 São José dos Campos, Brazil*

[6]*Instituto de Física Teórica, Universidade Estadual Paulista (UNESP), 01140-070 São Paulo, Brazil*

(Received 5 March 2016; published 3 October 2016)

Binary mixtures of Bose-Einstein condensates (BECs) trapped in deep optical lattices and subjected to equal contributions of Rashba and Dresselhaus spin-orbit coupling (SOC) are investigated in the presence of a periodic time modulation of the Zeeman field. SOC tunability is explicitly demonstrated by adopting a mean-field tight-binding model for the BEC mixture and by performing an averaging approach in the strong modulation limit. In this case, the system can be reduced to an unmodulated vector discrete nonlinear Schrödinger equation with a rescaled SOC tuning parameter α, which depends only on the ratio between amplitude and frequency of the applied Zeeman field. We consider the attractive interaction case and focus on the effect of the SOC tuning on the localized ground states. The dependence of the spectrum of the linear system on α has been analytically characterized. In particular, we show that extremal curves (ground and highest excited states) of the linear spectrum are continuous piecewise functions (together with their derivatives) of α, which consist of a finite number of decreasing band lobes joined by constant lines. This structure also remains in the presence of inter- and intra-species interactions, the nonlinearity mainly introducing a number of localized states in the band gaps. The stability of ground states in the presence of the modulating field has been demonstrated by real-time evolutions of the original (unaveraged) system. Localization properties of the ground state induced by the SOC tuning, and a parameter design for possible experimental observation, have also been discussed.

DOI: 10.1103/PhysRevA.94.043602

I. INTRODUCTION

Spin-orbit coupling (SOC), i.e., the intrinsic interaction between the particle dynamics and its spin, is a phenomenon known from the dawn of quantum mechanics, representing a major source of magnetic intra-atomic interaction. In solid-state physics, SOC plays an important role mainly in the magnetism of solids that are well described in terms of individual ions, as it is for the case for the rare-earth insulators, as well as in the study of energy bands of semiconductors in the vicinity of the extremal points where usually band splitting is induced. The relevance of SOC in this context is well known from pioneering works of Dresselhaus and Rashba [1–6] and from the many theoretical and experimental developments which originated from them. In particular, in the recent past few decades there has been a flourishing of interest in developments of materials with strong SOC for practical applications in the fields of topological insulators [7], spintronics [8], anomalous Hall effects [9], and quantum computation [10], among other possibilities.

In generic condensed-matter materials, however, SOC is rather weak and also very difficult to manage being largely superseded by the electrostatic interactions. The situation is quite different with ultracold atoms for which a variety of synthetic SOC can be induced and managed by external laser fields. In particular, SOC has been experimentally realized for binary mixtures of Bose-Einstein condensates (BECs), as reported in Refs. [11,12], and theoretically investigated in several papers. The flexibility of ultracold atomic systems in the control of the interactions and the different types of SOC implementations permit us to explore novel magnetic phenomena difficult to achieve with solid-state materials. In this regard, we can mention the existence of new superfluid phases with unusual magnetic properties [13,14], stripe modes [15], fractional topological insulators [16–18], new topological excitation such as Weyl [19] and Majorana [20] fermions, antiferromagnetic states [21], solitons [22–26], and gap solitons [27–29]. In these contexts the tunability of SOC plays a crucial role both for distinguishing different phases arising under variations of parameters and for understanding the mechanism underlying the phenomena as well as the interplay between SOC and the inter- and intra-atomic interactions (nonlinearity).

Recently a lot of attention has been devoted to the investigation of universal high-frequency behavior of periodically driven systems. The important consequences are dynamical stabilizations and the Floquet engineering of cold-atomic systems under temporal modulations of parameters of the systems [30]. One should also notice the number of theoretical [31] and experimental [32] studies on SOC tunability, which have been done for continuous BEC systems with equal Rashba and Dresselhaus terms, by using rapid time variations of the Raman frequency. In view of the relevance of SOC induced phenomena, it is interesting to explore SOC tunability also for different parameters' modulations and in the presence of discrete settings as the ones induced by the presence of deep optical lattices (OLs).

The aim of the present paper is to investigate the SOC tunability of a binary BEC mixture trapped in a quasi-one-dimensional deep optical lattice in the presence of a

time-dependent Zeeman field. In this respect, we consider a combination of Rashba and Dresselhaus SOC realized either by Raman coupling two hyperfine ground states as done in [11] or by using a tripod scheme [33,34]. The external Zeeman field is assumed to vary periodically in time, restricting mainly to the case in which the amplitude, Ω_1, and frequency, ω, of the modulation is very large (strongly modulation limit). The deepness of the OL is accounted for by adopting the tight-binding SOC model of the BEC mixture introduced in Ref. [35], which is in the form of a vector discrete nonlinear Schrödinger equation with time-dependent Zeeman field. We show that this model reduces to an effective time-averaged equation which has the same form as for the original unmodulated system, but with an effective SOC parameter rescaled by a factor $J_0(\alpha)$, where J_0 is the zeroth-order Bessel function and $\alpha \equiv 2\Omega_1/\omega$ is the tuning parameter.

The effect of the modulating field on the energy (chemical potential) spectrum is studied by exact analytical expressions in the absence of nonlinearity, while we recourse to direct real- and imaginary-time evolutions of the original system and to exact self-consistent numerical diagonalization of the averaged Hamiltonian system in the nonlinear case. In particular, we show that the ground-state curve of the linear system is a piecewise function of α consisting of equally spaced branches (lobes) centered around the relative minima of the energy (chemical potential) and joined by flat regions of constant μ. A similar result applies also to the highest excited extremal curve by symmetry arguments. In the presence of interactions, besides the removal of the degeneracy of extended states, a set of discrete localized levels appears in the forbidden zone of the underlying linear band-gap structure, which displays oscillatory behaviors in terms of the tuning parameter, with amplitudes that decrease as α is increasing.

In this paper, we mainly consider the attractive interaction case, focusing on the effect of the SOC tuning on the localized ground states. The existence of ground-state stationary discrete solitons is explicitly investigated both by means of exact diagonalizations of the averaged system and by direct imaginary-time evolutions of the original system. The stability of these states is demonstrated by real-time evolutions of the original (unaveraged) system. We also consider the effect of the SOC tuning on localization properties of the ground state, by showing that for fixed equal attractive inter- and intraspecies interactions there exists an optimal value of α for which the maximum localization of the wave function is achieved. This optimal tuning corresponds to the point where the separation of the ground-state level from the bottom of the linear band assumes its maximum value as a function of α. The existence and stability of stripelike soliton solutions are also demonstrated. We find that, within the range of the α parameter and nonlinearity for which these solutions exist, their behaviors are similar to the one obtained for stationary ground states. Finally, the possibility to observe these phenomena in real experiments is briefly discussed at the end.

The paper is organized as follows. In Sec. II, we introduce the model equations of a binary BEC mixture in a deep OL with SOC and modulating Zeeman fields and derive the averaged equations with rescaled SOC parameters. In Sec. III, we use the dispersion relation of the averaged linear system to investigate the properties of the ground and highest excited states as functions of the tuning parameter. In Sec. IV we study how the linear spectral properties are affected by the nonlinearity. In Sec. V we study the influence of the SOC tuning on discrete soliton ground states with respect to existence and stability, as well as localization properties. The stability of the results, under time integrations, is shown by considering full numerical simulation of ground-state wave functions for different parameter choices. Finally, in Sec. VI, we discuss possible experimental implementations and physical estimates and conclude by summarizing our results.

II. MODEL EQUATIONS, AVERAGING, AND SOC TUNED LINEAR SPECTRUM

The model equations for a BEC mixture in a one-dimensional (1D) geometry can be derived from a more general three-dimensional formalism by considering a trapping potential with the transversal frequency $\omega_\perp$ much larger than the longitudinal one, $\omega_\perp \gg \omega_{||}$. In the present case, the trap potential in the x direction is an optical lattice given by a periodic potential $V_{\rm OL}(x) \sim \sin^2(k_L x)$, where k_L is the lattice wave number. In the mean field approximation, the system is described by a 1D Gross-Pitaevskii (GP) coupled equation for the two-component wave function, $\Psi \equiv \Psi(x,t)$, which is normalized to the total number, N, of atoms, as

$$\Psi \equiv \begin{pmatrix} \Psi_1 \\ \Psi_2 \end{pmatrix}, \quad \sum_{j=1}^{2} \int dx |\Psi_j|^2 = N. \tag{1}$$

In the presence of SOC the corresponding GP formalism is given by the following 1D Hamiltonian, with two terms. The first term, H_0, is linear and includes the SOC and optical lattice. The other term, given by $H_{\rm NL}$, is nonlinear and includes the two-body atomic interactions [21,27,36]. In matrix form, it can be written as

$$\begin{aligned} i\hbar \frac{\partial \Psi}{\partial t} &= [H_0 + H_{\rm NL}]\Psi, \\ H_0 &\equiv \frac{P_x^2}{2m} + \frac{\hbar\kappa}{m} P_x \sigma_x + V_{\rm OL}(x) + \hbar\overline{\Omega}\sigma_z, \\ H_{\rm NL} &\equiv 2\hbar\omega_\perp \begin{pmatrix} \sum_j a_{1j}|\Psi_j|^2 & 0 \\ 0 & \sum_j a_{j2}|\Psi_j|^2 \end{pmatrix}, \end{aligned} \tag{2}$$

where $\sigma_{x,z}$ are the usual Pauli matrices, a_{jj} $(j = 1,2)$ and a_{12} are the two-body scattering lengths between intra- and interspecies of atoms, and the parameter $\overline{\Omega}$ is defined by detuning or by the external Zeeman field. The above formalism, Eqs. (1) and (2), can be written as

$$\begin{aligned} i\hbar \frac{\partial \Psi_j}{\partial t} &= \left[-\frac{\hbar^2}{2m}\frac{\partial^2}{\partial x^2} + V_{\rm OL}(x) - (-)^j \hbar\overline{\Omega} \right] \Psi_j \\ &\quad + 2\hbar\omega_\perp (a_{jj}|\Psi_j|^2 + a_{j,3-j}|\Psi_{3-j}|^2)\Psi_j \\ &\quad - i\frac{\hbar^2\kappa}{m}\frac{\partial \Psi_{3-j}}{\partial x}, \quad (j = 1,2). \end{aligned} \tag{3}$$

The form of SOC corresponding to this GP system can be obtained by coupling two hyperfine states $|F = 1, m_F = 0\rangle$ and $|F = 1, m_F = -1\rangle$, with the state $|F = 1, m_F = +1\rangle$ far detuned from the others, by means of a pair of Raman laser beams, as implemented for the ^{87}Rb condensate in

the seminal work [11]. The SOC system considered in this work is equivalent to Eq. (3) upon a pseudo-spin-rotation $\sigma_x \to -\sigma_z$ and $\sigma_z \to \sigma_x$, such that the Rashba and Dresselhaus SOCs have equal strength [37]. Alternatively, it is possible to use a tripod scheme for the generation of synthetic gauge fields [33,34]. In this case, the scheme operates with atoms in three degenerated ground states ($|i\rangle, i = 1,2,3$) coupled to a common excited state ($|e\rangle$) by three laser beams. The optical lattice, given by $V_{\rm OL}(x) \equiv V_0 \cos(2k_L x)$, can be generated by two counterpropagating laser fields. For a dimensionless formalism, we make the following replacements in Eq. (3):

$$\begin{aligned} x \to \frac{x}{k_L}, \quad t \to \frac{t}{\omega_R}, \quad \text{where } \omega_R \equiv \frac{E_R}{\hbar} \equiv \frac{\hbar k_L^2}{2m}; \\ V_{\rm OL}(x) \to E_R V(x) = E_R V_0 \cos(2x), \\ \Psi_j \equiv \sqrt{\frac{\omega_R}{2\omega_\perp a_0}}\psi_j(x,t), \end{aligned} \tag{4}$$

with the definitions

$$b \equiv \frac{2\kappa}{k_L}, \quad \Omega = \frac{\overline{\Omega}}{\omega_R}, \quad g_j = \frac{a_{jj}}{a_0}, \quad g = \frac{a_{j,3-j}}{a_0}. \tag{5}$$

In the above E_R is the recoil energy and a_0 is the background scattering length. Therefore, with $\psi_j \equiv \psi_j(x,t)$, we obtain

$$\begin{aligned} i\frac{\partial \psi_j}{\partial t} = \left[-\frac{\partial^2}{\partial x^2} + V(x) - (-)^j \Omega\right]\psi_j - ib\frac{\partial \psi_{3-j}}{\partial x} \\ + (g_j|\psi_j|^2 + g|\psi_{3-j}|^2)\psi_j, \quad (j = 1,2). \end{aligned} \tag{6}$$

From Eqs. (5) and (1), the total number of atoms can be written as

$$N = \frac{\omega_R}{2\omega_\perp k_L a_0}\sum_{j=1}^{2}\int dx|\psi_j|^2 \equiv \frac{\omega_R \overline{N}}{2\omega_\perp k_L a_0}, \tag{7}$$

with $\overline{N}$ the rescaled number of atoms (norm).

A BEC system with a spin-orbit coupling as shown by the above formalism, when loaded in a deep optical lattice, can be described in the tight-binding model with mean-field approximation, by the following system for the discrete nonlinear Schrödinger equation with SOC (SOC-DNLS) [35]:

$$\begin{aligned} i\frac{du_n}{dt} &= -\Gamma(u_{n+1} + u_{n-1}) + i\frac{\chi}{2}(v_{n+1} - v_{n-1}) \\ &\quad + \Omega u_n + (\gamma_1|u_n|^2 + \gamma|v_n|^2)u_n, \\ i\frac{dv_n}{dt} &= -\Gamma(v_{n+1} + v_{n-1}) + i\frac{\chi}{2}(u_{n+1} - u_{n-1}) \\ &\quad - \Omega v_n + (\gamma|u_n|^2 + \gamma_2|v_n|^2)v_n, \end{aligned} \tag{8}$$

where

$$\begin{aligned} \Gamma \equiv \Gamma_{n,n+1} = \int w^*(x-n)\frac{\partial^2}{\partial x^2}w(x-n-1)dx, \\ \gamma = \mathrm{g}\int |w(x-n)|^4 dx,\ \gamma_i = \mathrm{g}_i \int |w(x-n)|^4 dx, \\ \chi \equiv \chi_{n,n+1} = 2b\int w^*(x-n)\frac{\partial}{\partial x}w(x-n-1)dx. \end{aligned} \tag{9}$$

Notice that Eq. (8) has two conserved quantities: the norm,

$$\overline{N} = \sum_n (|u_n|^2 + |v_n|^2), \tag{10}$$

and the Hamiltonian (energy)

$$\begin{aligned} E \equiv H = \sum_n \Big\{ -\Gamma(u_n^* u_{n+1} + v_n^* v_{n+1}) + i\frac{\chi}{2}u_n^*(v_{n+1} - v_{n-1}) \\ + \frac{\Omega_0}{2}(|u_n|^2 - |v_n|^2) + \text{ c.c.}\Big\} + E_{\rm int}, \end{aligned} \tag{11}$$

where $E_{\rm int}$ is the interaction energy,

$$E_{\rm int} = \sum_n \left\{\tfrac{1}{2}(\gamma_1|u_n|^4 + \gamma_2|v_n|^4) + \gamma|u_n|^2|v_n|^2\right\}, \tag{12}$$

and c.c. denotes the complex conjugate of the expression in the curly bracket. Next, in order to achieve a tunable SOC, we assume that the Zeeman field is periodically varying in time, as

$$\Omega = \Omega(t) = \Omega_0 + \Omega_1 \cos(\omega t), \tag{13}$$

where Ω_0 is the fixed constant part of the field and Ω_1 is the amplitude of the part modulated with frequency ω. In view of this time dependence of the Zeeman field, given by Eq. (13), it is convenient to express the coupled system (8) by an effective time-averaged system, which can be implemented by the following transformation:

$$u_n = U_n e^{-i\beta(t)}, \quad v_n = V_n e^{+i\beta(t)}, \tag{14}$$

where

$$\beta(t) = \Omega_1 \int_0^t \cos(\omega\tau)d\tau = \frac{\Omega_1}{\omega}\sin(\omega t). \tag{15}$$

Once the transformation (14) is made, the coupled Eq. (8) can be rewritten, such that the explicit time dependence is removed from the Zeeman field (remaining only the constant term Ω_0), being transferred to the constant χ, which has to be replaced by $\chi \exp[2i\beta(t)]$.

Next, we perform the time averaging of Eq. (8), over the period ($T = 2\pi/\omega$) of the rapid oscillation, by using that

$$\frac{1}{2\pi}\int_0^{2\pi} d(\omega t)\exp\left(\frac{2i\Omega_1}{\omega}\sin(\omega t)\right) = J_0\left(\frac{2\Omega_1}{\omega}\right), \tag{16}$$

where $J_0(\alpha)$ is the zeroth-order Bessel function in the variable α. The above averaging procedure applied to Eq. (8) leads to the following coupled system:

$$\begin{aligned} i\frac{dU_n}{dt} &= -\Gamma(U_{n+1} + U_{n-1}) + i\frac{\chi J_0(\alpha)}{2}(V_{n+1} - V_{n-1}) \\ &\quad + \Omega_0 U_n + (\gamma_1|U_n|^2 + \gamma|V_n|^2)U_n, \\ i\frac{dV_n}{dt} &= -\Gamma(V_{n+1} + V_{n-1}) + i\frac{\chi J_0(\alpha)}{2}(U_{n+1} - U_{n-1}) \\ &\quad - \Omega_0 V_n + (\gamma|U_n|^2 + \gamma_2|V_n|^2)V_n. \end{aligned} \tag{17}$$

Quite remarkably, we see that the time-averaged system given in Eq. (17) coincides with Eq. (8) under the following replacement:

$$\Omega \to \Omega_0, \quad \chi \to \chi_{\rm eff} \equiv \chi J_0(\alpha), \quad \alpha \equiv \frac{2\Omega_1}{\omega}. \tag{18}$$

Strictly speaking, these averaged equations are valid only in the strong modulation limit, e.g., when Ω_1 and ω are both very large with their ratio being finite. However, we shall see later that their validity extends in a wide range away from this limit.

In the next two sections we study the spectral properties of the SOC system by diagonalizing the eigenvalue problem obtained from the discrete coupled Schrödinger equation (17) when we consider stationary solutions of the form

$$U_n(t) = e^{-i\mu t}U_n, \quad V_n(t) = e^{-i\mu t}V_n, \tag{19}$$

where μ denotes the chemical potential. Notice that from Eqs. (8) and (11) it readily follows that μ is related to the energy E and to the number of atoms by the following relation:

$$\mu N = E + E_{\rm int}, \tag{20}$$

with $E_{\rm int}$ given by Eq. (12). Also notice that for the linear system the chemical potential coincides with the energy per particle, e.g., $\epsilon \equiv E/N = \mu$.

III. SPECTRAL PROPERTIES OF THE SOC TUNED LINEAR SYSTEM

In the absence of any interaction, e.g., for $\gamma_1 = \gamma_2 = \gamma = 0$, the averaged system given by Eq. (17) becomes exactly solvable and the dispersion relation can be given analytically. Indeed, from Eq. (18) we have that the linear dispersion relations of the modulated system simply follow from the ones of the unmodulated system given in [35,38], as

$$\mu(k,\alpha)_{\pm} = -2\Gamma\cos(k) \pm \sqrt{\Omega_0^2 + [\chi J_0(\alpha)]^2 \sin^2(k)}, \tag{21}$$

with k, the crystal momentum, varying in the first Brillouin zone $k \in [-\pi,\pi]$. The minus and plus signs refer to the lower and upper parts of the dispersion curves (bands) in the reciprocal space, respectively. In Fig. 1 we depict the linear dispersion curves obtained from Eq. (21) for three different values of the tuning parameter α.

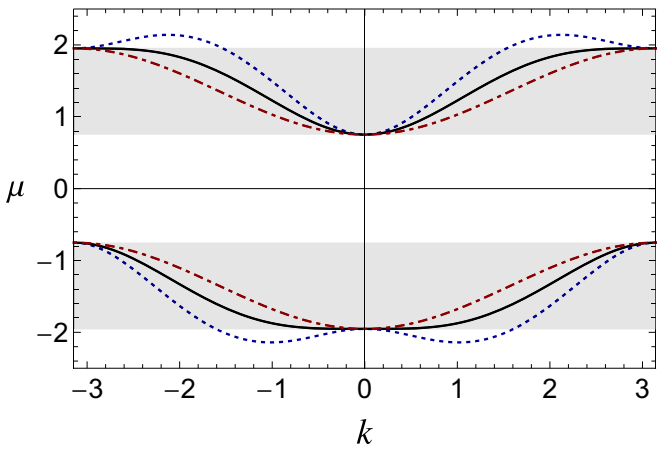

FIG. 1. Dispersion curves of the SOC-DNLS system for the linear case ($\gamma_1 = \gamma_2 = \gamma = 0$), with three different modulational parameters: $\alpha = 0.4$ (dotted-blue curves), $\alpha = 1.33734$ (continuous curves), $\alpha = 2.5$ (dot-dashed-red curves). Other parameters are fixed as $\Gamma = 0.3$, $\Omega_0 = 1.352$, $\chi = 1.5$. Shadowed regions indicate the linear bandwidths for values of $\alpha \geqslant \alpha_0^+$, where $\alpha_0^+ \approx 1.33734$ is the critical value in Eq. (25), at which the local extremal points coalesce. Plotted quantities are in normalized units.

Starting from Eq. (17), the behavior of the linear spectrum as a function of the tuning parameter α can be further investigated. In this respect, notice from Eq. (21) that the dispersion curves have two degenerate extremal points at positions

$$k_s(\alpha) = \cos^{-1}\left[-s\frac{2\Gamma}{\chi J_0(\alpha)}\sqrt{\frac{\Omega_0^2 + [\chi J_0(\alpha)]^2}{4\Gamma^2 + [\chi J_0(\alpha)]^2}}\right] \tag{22}$$

with $s = \pm 1$.

As the chemical potential for k_s is given by

$$\mu_s \equiv \mu(k_s,\alpha) = \frac{s\sqrt{\left[\chi^2 J_0^2(\alpha) + 4\Gamma^2\right]\left[\chi^2 J_0^2(\alpha) + \Omega_0^2\right]}}{\chi J_0(\alpha)}, \tag{23}$$

the solutions at the extremal points are obtained from

$$\frac{d\mu_s}{d\alpha} = \frac{s}{\chi J_0^2(\alpha)}\frac{J_1(\alpha)\left[\chi^4 J_0^4(\alpha) - 4\Gamma^2\Omega_0^2\right]}{\sqrt{\left[\chi^2 J_0^2(\alpha) + 4\Gamma^2\right]\left[\chi^2 J_0^2(\alpha) + \Omega_0^2\right]}} = 0, \tag{24}$$

which are at $\alpha_i = \alpha_i^{\pm}$ $(i = 0,1,2,...)$, given by

$$J_0(\alpha_i^{\pm}) = \pm\frac{\sqrt{2\Gamma\Omega_0}}{\chi} \tag{25}$$

and, at $\alpha = \eta_n$ $(n = 0,1,2,...)$, for

$$J_1(\eta_n) = 0. \tag{26}$$

A typical dependence of the linear spectrum as a function of the tuning parameter α is depicted in Fig. 2. In this figure, shown is only part of the spectrum corresponding to the lower band, since the part corresponding to the upper band can be obtained from specular reflection with respect to the $\mu = 0$ axis. Notice that different curves correspond to different values of k and the spectrum for a given α covers the first band in the whole Brillouin zone $k \in [-\pi,\pi]$.

From Fig. 2 one can directly verify that the conditions given above are satisfied at the zeros of $J_1(\alpha = \eta_n)$, given by Eq. (26), and for the possible solutions $\alpha_i^{\pm}$ of $J_0(\alpha)$, given by Eq. (25). It is also easy to check that for each η_i, $i = 1,2,3,\ldots$, there exist satellite solutions α_i^-, α_i^+ of Eq. (25) lying immediately before and after η_i and equidistant from it, e.g., $\eta_i = (\alpha_i^+ + \alpha_i^-)/2$, while for the point $\eta_0 = 0$ there exists only the upper satellite α_0^+. Thus, for all $\alpha \in R^+$ (notice that the dispersion relation is symmetric in α), the sequence α^* of all extremal points resulting from the above equations can be put in increasing order as follows:

$$\alpha^* \equiv \{0,\alpha_0^+,\alpha_1^-,\eta_1,\alpha_1^+,\alpha_2^-,\eta_2,\alpha_2^+,...,\} \tag{27}$$

and thus the dependence on α of the extremal μ_- curve can be separately investigated for the sequence of nonoverlapping intervals

$$I_{\eta_0} = [0,\alpha_0^+], \quad I_{\eta_i} = [\eta_i - \Delta_i, \eta_i + \Delta_i], \; i = 1,2,\ldots,$$
$$I_{\alpha_i} =]\alpha_i^+,\alpha_{i+1}^-[, \; i = 0,1,2,\ldots \tag{28}$$

with $\Delta_i = (\alpha_i^+ - \alpha_i^-)/2$.

One can prove that the chemical potential assumes a constant value $\mu_- = -2\Gamma - \Omega_0$ at the satellite points $\alpha_i^{\pm}$

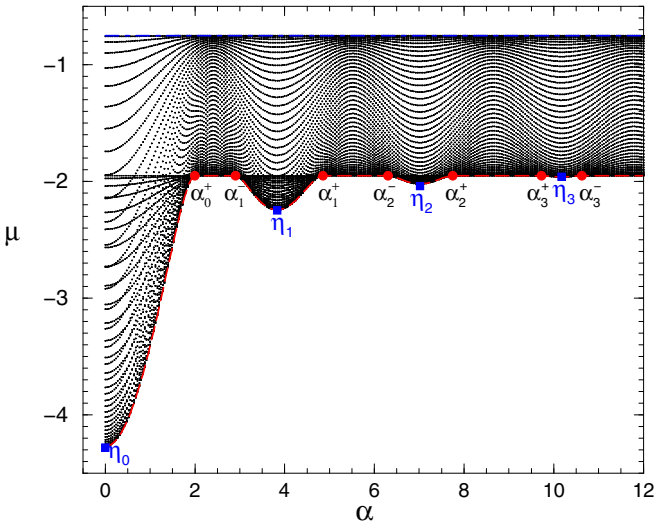

FIG. 2. Lower-band spectrum of chemical potential as a function of α for a SOC-DNLS chain of 99 sites in the linear limit $\gamma_1 = \gamma_2 = \gamma = 0$, for $\chi = 4.0$, with other parameters fixed as in Fig. 1. The dashed-red curve displays the ground-state dependence, while the top dot-dashed-blue line corresponds to the lower limit of the interband gap. For the chosen parameters we can identify one half lobe started at the origin (with minimum at η_0, going till α_0^+) and three other lobes (with minima at η_1, η_2, and η_3), where the last one is hardly visible in the given plot scale. Red bullets and blue squares correspond to values of α given by Eqs. (25) and (26), with $\alpha_0^+ = 1.9978$, $\alpha_1^- = 2.9023$, $\alpha_1^+ = 4.8504$, $\alpha_2^- = 6.3065$, $\alpha_2^+ = 7.7503$, $\alpha_3^- = 9.7298$, and $\alpha_3^+ = 10.6238$. Plotted quantities are in normalized units.

and inside all the intervals I_{α_i} $i = 0,1,2,\ldots$. This directly follows from Eq. (21) and from the fact that inside the intervals I_{α_i} the quasimomentum $k_s(\alpha)$ becomes complex so that the only physical acceptable solutions for μ_- are the ones independent on α, e.g., the ones for which $k = 0, \pm\pi$ giving $\mu = -2\Gamma \pm \Omega_0$ and $2\Gamma \pm \Omega_0$, respectively. Notice that, while the values $-2\Gamma - \Omega_0$ and $2\Gamma + \Omega_0$ correspond, respectively, to the ground and to the highest excited states of the chemical potential in the regions I_α, the other two constants $-2\Gamma + \Omega_0$ and $2\Gamma - \Omega_0$ are delimiting the lower and upper borders of the inter-band gap. From this it follows that the lower and upper extremal curves are flat for all $\alpha \in I_{\alpha_i}$. It is worth noting that in terms of the dispersion curves in the reciprocal space the critical values $\alpha_i^\pm$ also correspond to the values of α for which the two minima (maxima) k_{-1} (k_1) of the lower (upper) band coalesce into a single minimum (maximum), at $k = 0$ ($k = \pi$). This is pictorially illustrated in Fig. 1 where the linear dispersion curves are depicted for different values of the tuning parameter α.

On the other hand, in the I_{η_i} intervals, the dependence of the chemical potential on α gives continuous local extremal curves, referred to in the following as "lobes," which are symmetric around their minimum at $\alpha = \eta_i$. The amplitudes of the lobes decrease as α is increased, the absolute minimum being attained at $\alpha = 0$ where a half lobe is observed (notice that due to the parity of μ on α we can restrict only to non-negative values of α, meaning that the lobe around $\alpha = \eta_0 = 0$ becomes a half lobe).

Also note that the lobe profiles tangentially intersect the horizontal line $-2\Gamma - \Omega_0$ at the borders of the I_{η_i} intervals. From this it follows that the ground-state curve and its derivative are both continuous functions of α. These properties can be directly checked by plotting the curves $\mu_-(k_s,\alpha)$ in the interval I_{η_i}, with $s = (-1)^{i+1}$ for the ith lobes, $i = 0,1,2,\ldots$.

Thus, from the above analysis we conclude that the ground state of the linear system is a continuous piecewise function of α which consists of a finite number of equally spaced lobes at $\alpha = \eta_i$ (half lobe at $\alpha = 0$) joined by the constant line $\mu_- = -2\Gamma - \Omega_0$ inside the I_{α_i} intervals. It can be proved that, for fixed values of the parameters, the number of lobes in the ground-state curve (e.g., excluding the half lobe at the origin) is given by the maximal integer, $i_{\max}$, for which the quasimomentum $k_s(\eta_{i_{\max}})$, with $s = (-1)^{i_{\max}+1}$, is still real. Therefore, the sequence of intervals in Eq. (28) is finite, with the last $I_{\alpha_{i_{\max}}}$ flat interval given by $]\alpha_{i_{\max}},\infty]$.

Similar results follow by symmetry arguments also for the highest excited extremal curve $\mu_+(\alpha^*)$. In this case $\mu_+ = 2\Gamma + \Omega_0$ at satellite points, lobes have maxima at η_i and tangentially intersect the constant line $2\Gamma + \Omega_0$ of intervals I_{α_i}. Since the lower and upper border of the inter-band-gap are constant in α, we also have that the lower band linear spectrum is constrained inside the lower extremal (ground state) curve and the lower gap border $-2\Gamma + \Omega_0$ (similarly, the upper band spectrum lies between the upper gap border $2\Gamma - \Omega_0$ and the highest excited state extremal curve). In the next section we shall see that some of the linear features survive also in the presence of nonlinearity.

IV. SOC TUNED NONLINEAR SPECTRUM

Spectral properties of the nonlinear system have been obtained from self-consistent exact diagonalization of the averaged Hamiltonian system (17). The numerical approach is described in more details in Ref. [39] for the single component case, with extension to the multicomponent case being straightforward. In all numerical calculations performed in the nonlinear case we always rescaled the wave-function components and the nonlinear coefficients in Eq. (8) according to

$$u_n \to \frac{u_n}{\sqrt{N}}, \quad v_n \to \frac{v_n}{\sqrt{N}}, \tag{29}$$

$$\gamma \to \gamma N, \quad \gamma_i \to \gamma_i N, \quad i = 1,2, \tag{30}$$

such that the total wave function is normalized to 1:

$$\sum_n (|u_n|^2 + |v_n|^2) = N_u + N_v = 1. \tag{31}$$

In the top panels of Fig. 3 we depict the spectrum of the energy per particle ϵ vs the tuning parameter α, as obtained in the nonlinear cases for $\gamma = -0.2$ (left panels) and $\gamma = -0.8$ (right panels), considering all equal, $\gamma_1 = \gamma_2 = \gamma$, attractive interactions. The spectrum shown in the top-left panel, with $\gamma = -0.2$, is quite similar to the linear case, with the eigenvalues oscillating as functions of the tuning parameter, and with amplitudes decreasing as α is increased. One should notice that only one lobe at the origin appears for this set of parameters with $\chi = 1.5$, in contrast with the linear case shown in Fig. 2, with $\chi = 4.0$, where other lobes can be identified at the zeros of $J_1(\alpha)$, given by Eq. (26). In the level of

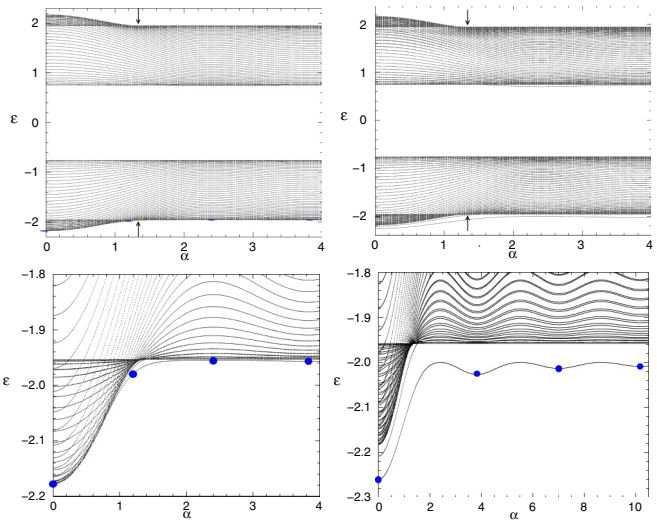

FIG. 3. Energy spectrum of the averaged SOC-DNLS system vs α for a chain with 99 sites, with $\gamma = -0.2$ (left panels) and $\gamma = -0.8$ (right panels). In both cases, the full spectra are in the top panels with corresponding lower part in the bottom panels. The arrows in the top panels indicate the critical point $\alpha_0^+ = 1.33734$ at which the linear bandwidths becomes uniform [see also Fig. 1 and Eq. (25)]. The other parameters are fixed as $\Gamma = 0.3$, $\Omega_0 = 1.352$, and $\chi = 1.5$. Notice that for these parameters only the half lobe in the origin exists. The blue bullets on top of the ground-state curves in bottom panels are related to the wave functions shown in Figs. 5 (right panel) and 6 (left panel). Plotted quantities are in normalized units.

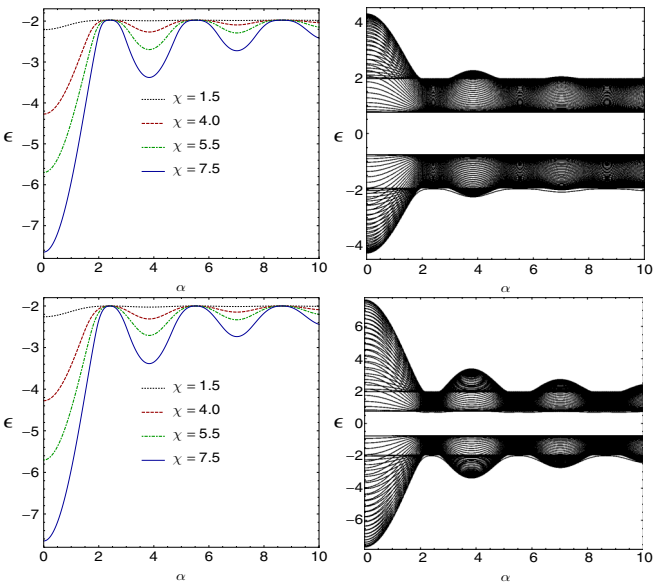

FIG. 4. Left panels: Ground-state energies as functions of the tuning parameter $\alpha = 2\Omega_1/\omega$ for different values of χ (indicated inside the panels), with unequal, $\gamma_1 = -0.4, \gamma_2 = -0.6, \gamma = -0.1$ (top panel), and with all equal, $\gamma_1 = \gamma_2 = \gamma = -0.8$ (bottom panel), nonlinearities. Other parameters are fixed as in Fig. 3. Right panels: Full spectrum vs α for $\chi = 4.0$ (top) and $\chi = 7.5$ (bottom) with other parameters fixed as in the corresponding left panel. Plotted quantities are in normalized units.

the oscillations, the positions of the extremal points (maxima or minima) observed in the lower and upper bands are in direct correspondence with the zeros of the Bessel function, $J_0(\alpha)$, and its first derivative, $J_1(\alpha)$. More explicitly, for the case shown in the top-right panel, one can identify more clearly the corresponding ground state in the lower band, which is given in the lower-right panel of Fig. 3. The observed minima are close to $\alpha = 0$, 3.83, 7.02, 10.17 [zeros of $J_1(\alpha)$], with the maxima close to $\alpha = 2.405$, 5.52, 8.65 [zeros of $J_0(\alpha)$].

We also observe that the upward (downward) rearrangement of the levels gives rise to the half lobe of the nonlinear spectrum when the tuning parameter is varied in the region $0 < \alpha \leqslant \alpha_0^+$, where $\alpha_0^+ = 1.33734$ is practically the same value expected for the linear spectrum. Notice, however, that the nonlinearity introduces localized states in the band gaps (this occurring at first order in the perturbation while effects on band levels are typically of higher orders). Except for this, the qualitative behavior of the spectral oscillations (lobes) in the presence of nonlinearity can be qualitatively understood from the analysis performed in the previous section. In particular, note from Eq. (21) and from the crossover of the linear bands across the critical point in Eq. (25) that, for $\alpha < \alpha_0^+$, there are points of the spectrum lying outside the shadowed region of Fig. 1. These points correspond to the upper and lower band half lobes observed in the top panels of Fig. 3 (for the chosen parameters the linear spectrum has only the half lobe at the origin and the flat semi-infinite interval $]\alpha_0^+, \infty]$). However, for $\alpha \geqslant \alpha_0^+$, all points lie inside the shadowed region corresponding to the flat curves shown in Fig. 3, in full agreement with the analysis of the linear system, in spite of the presence of the nonlinearity.

Spectral modulations induced by the Zeeman term in the presence of nonlinearity are clearly visible in the bottom panels of Fig. 3 for two different sets of nonlinearity parameters. As shown, in these cases the main difference is the appearance of isolated levels in the gaps. The spectral oscillations inside the bands persist in the presence of nonlinearity, with the ground-state curve oscillating in phase with curves of excited levels inside the lower band.

The effects of the nonlinearity on the ground-state energy and on the full spectrum are further investigated as functions of α in Fig. 4. In particular, in the left panels of this figure we show ground-state behaviors for different values of the spin-orbit parameter χ, with two different choices of the nonlinear parameters corresponding to attractive interactions. In the upper-left panel we have all unequal interactions and, in the lower-left panel, all the interaction parameters are the same. The full spectra with respect to α, for two specific values of χ, with all other parameters as in the corresponding left panels are shown in the right panels of Fig. 4. From this figure, we notice that the behaviors for "all equal" and "all unequal" interactions are qualitatively similar, this being particularly true if nonlinearities are not too large. Moreover, the amplitudes of the oscillations increase with the increasing of χ, as verified for the ground state, which is a natural consequence of the χ dependence on the rescaling (18). Notice the existence of points where a localized level in the semi-infinite gap touches a band lobe (say, the ith lobe), with subsequent detachment at a point α symmetrically located with

respect to η_i (this being particularly visible for the first lobe of the $\chi = 7.5$ spectrum). The localization of the ground state changes rapidly at such points, passing from a well-localized state inside the gap to a nonlinear stripelike extended state bordering the lobe band (see bottom right panel of Figs. 4 and 9 below).

In conclusion, as far as the nonlinear spectrum is concerned, we can say that the main role of the nonlinearity is to introduce localized states in the gap, which display very interesting change of properties when they undergo collisions with the band lobes. Remarkably, the structure of the extremal curves (including the gap) of the linear band is well preserved also in the presence of intermediate (not too large) values of the nonlinearity (for instance, compare the top right panel of Fig. 4 with Fig. 2).

With respect to the localized states in the band gaps, they refer to discrete versions of gap solitons of the continuous BEC mixtures in OLs. Their existence is related to the modulational instability of linear Bloch states [40], a well-known phenomenon that we are not discussing here. Existence and stability of SOC tunable discrete solitons will be instead investigated in the next section by numerical methods. In view of the qualitatively similar results observed for different nonlinearity values, in the rest of this paper we refer only to attractive and all equal magnitude interactions.

V. SOC TUNED DNLS SOLITONS

In this section we consider effects of the SOC tuning on the existence, stability, and localization properties of stationary solitonic ground states and stripe solutions of both averaged and original (e.g., with time modulated Zeeman term) systems. In this regard, we recourse to numerical methods which we briefly describe here. For the averaged system, besides the self-consistent numerical diagonalization to obtain spectral properties discussed in the previous section, we also consider the relaxation method based on imaginary-time evolution [41] with a fourth-order Runge-Kutta (RK) method to obtain the ground-state wave functions, with periodic boundary conditions. Notice that in the imaginary-time evolution, and in all our numerical calculations, the components u_n and v_n of the eigenstates are normalized according to Eq. (31). The results obtained with imaginary-time propagation were found in perfect agreement with the ones obtained by self-consistent method and presented in Fig. 3 for the ground state.

Real-time evolution is also performed with the same RK code, with time step up to 10^{-4}, and the same periodic boundary conditions. During the real-time evolution, the conservation of the total norm was always monitored to check the accuracy.

In the upper-block panels of Fig. 5 we depict the stationary ground states of the averaged system in correspondence of the four local minima $\alpha = \eta_i$ ($i = 0,1,2,3$) represented in the energy curve displayed in the bottom-right panel of Fig. 3. As expected, for attractive interactions these ground states are found to be stable under time integrations of the averaged equation Eq. (17), as well as under time evolutions of the full system, with $\Omega_1 = 100$ and ω fixed according to the given value of α. In Fig. 5, the stability under time evolution is evidenced in the corresponding lower-block panels, where we

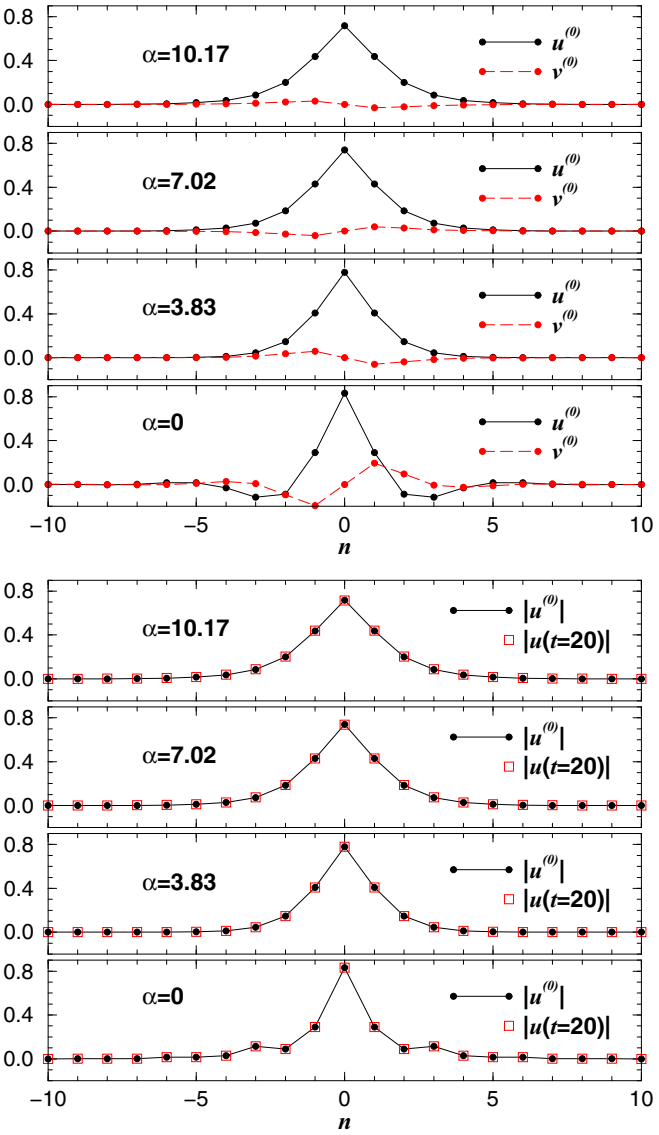

FIG. 5. Ground-state wave functions related to the four minima depicted in the right-lower panel of Fig. 3, corresponding to the zeros of $J_1(\alpha)$ (given inside the panels). In the upper block of panels we have the u (pure real) and v (pure imaginary) components. In the right lower block of panels, we indicate the time stability of the results by considering just the module of the u component, for $t = 0$ and 20. The parameters are as in the right frames of Fig. 3, with $\Omega_1 = 100$, $\Omega_0 = 1.352$, $\gamma = -0.8$, $\Gamma = 0.3$, and $\chi = 1.5$. The wave function is normalized as in Eq. (31), with the respective number fractions of the u component given by $N_u = 0.9056, 0.9897, 0.9950$, and 0.9967. Plotted quantities are in normalized units.

show results for the absolute values of the u component, considering $t = 0$ and 20. Notice, from the corresponding panels of the blocks, the change of internal phase of the wave function at different minima, with the tendency to become more localized at small values of the tuning parameter, expanding as α increases. It is worth remarking that maxima of the oscillating part of the ground-state curves are in correspondence to the Bessel function J_0 zeros. Therefore, they correspond to the vanishing of the rescaled SOC parameter. Ground-state profiles at these points are obviously

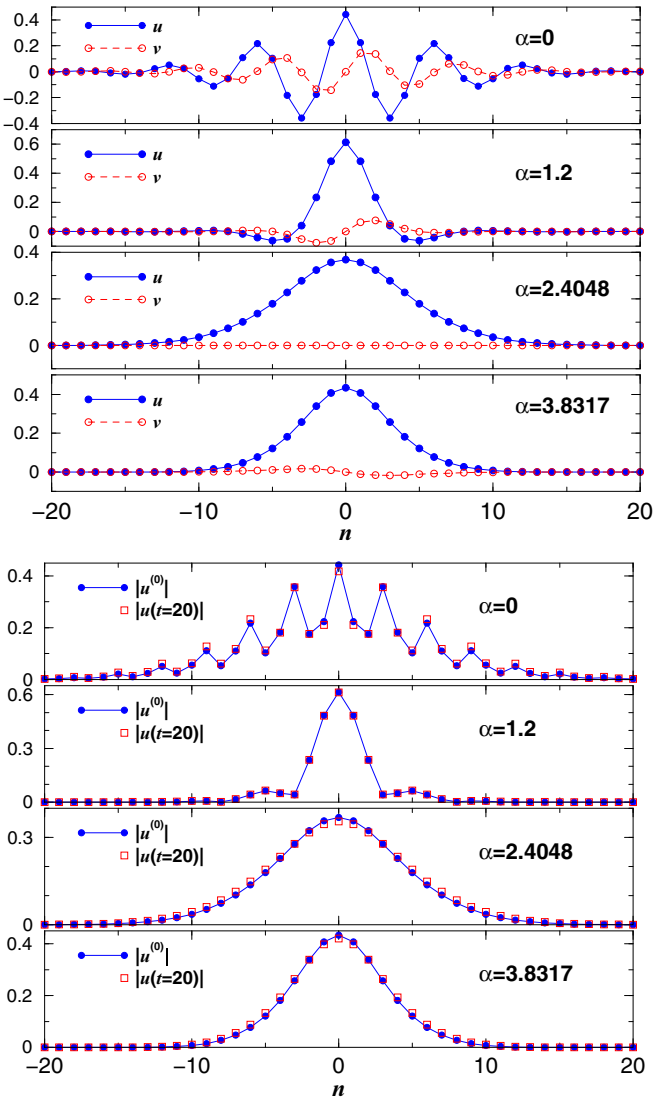

FIG. 6. Ground-state wave functions corresponding to the four dots depicted in the left-lower panel of Fig. 3, for the α values indicated inside the frames. In the upper block of panels we have the components u (solid blue) and v (dashed red). In the lower block of panels, the time stability is indicated by considering the module of u for $t = 0$ and 20. The parameters are as in the left frames of Fig. 3, with $\Omega_1 = 100$, $\Omega_0 = 1.352$, $\gamma = -0.2$, $\Gamma = 0.3$, and $\chi = 1.5$. Plotted quantities are in normalized units.

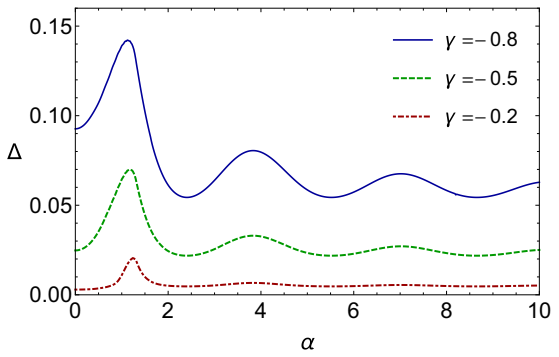

FIG. 7. Ground-state gap energy, $\Delta \equiv \epsilon_1 - \epsilon_0$, as a function of the tuning parameter α, for different attractive interactions γ indicated inside the frame. The maximum gap energy occurs at $\alpha = 1.12$ ($\Delta_{\max} = 0.142$), $\alpha = 1.18$ ($\Delta_{\max} = 0.07$), and $\alpha = 1.24$ ($\Delta_{\max} = 0.02$), for curves $\gamma = -0.8, \gamma = -0.5, \gamma = -0.2$, respectively. Other parameters are fixed as in Fig. 3. Plotted quantities are in normalized units.

less localized, since their chemical potentials have minimal distance from the linear band. In contrast, for $\alpha = 0$ we have $J_0(\alpha) = 1$, having the largest value of the SOC parameter. One could expect the state to be more localized at this point. The maximal localization, however, is achieved somewhere between $\alpha = 0$ and the first zero of J_0 as a result of the interplay between SOC and nonlinearity. Similar behaviors are found also for a different (lower) value of the nonlinearity as one can see from the panels of Fig. 6, corresponding to the ground-state curve shown in the bottom left panel of Fig. (3). As one can observe from Figs. 5 and 6, the maximal localization is also achieved at the intermediate value $\alpha \approx 1.25$.

In order to better quantify the influence of the SOC modulation on the ground-state localization, we have depicted in Fig. 7 the behavior of the ground-state gap energy, Δ, as a function of α for three different values of the interatomic interaction parameter γ, where Δ is defined as the difference between the ground state and the first excited state of the lower band. We observe that, for $\gamma = -0.2$, the maximum gap is achieved for $\alpha \approx 1.23$, in correspondence to the intermediate value between $\alpha = 0$, where the SOC parameter is maximum, and $\alpha = \eta_1$, where the corresponding ground-state curve has its first local minimum.

One should also observe that, as it is natural to expect for attractive interactions, the gap Δ increases as the interatomic interaction increases, but the relative weight of the peak at $\alpha \approx 1.3$ becomes more pronounced at small nonlinearities. The peak is a consequence of the interplay of SOC and the nonlinear interactions. Since at the largest value of Δ the energy of the ground state is more detached from the linear band, it is clear that at this value one expects the maximal localization to occur. For the chosen parameters, this is achieved at $\alpha \approx 1.2$, with a very small dependence on the interaction parameter γ, as one can see from Fig. 7. A similar behavior is found also for the excited localized wave functions inside the inter-band-gap; however, we do not pursue the analysis of these states here, because they appear to be unstable under time evolution.

We have also investigated the range of validity of the averaged equations away from the strong modulation limit, with results presented in Fig. 8. In this respect, we consider, for a fixed value of α, the original time modulated system with different oscillation amplitudes Ω_1, ranging from very large to relatively small values, with the corresponding frequency ω fixed by the chosen α. We use the exact solution of the averaged system as initial condition to start the time propagation under Eq. (8). Typical stability results for the absolute values of the ground-state components u and v are illustrated in Fig. 8, by considering three fixed values of Ω_1 (=10, 20, and 100), with the time evolution being performed from $t = 0$ to 20. As one can see, the results for $t = 20$ start to deviate from the original one when we have $\Omega_1 = 10$ (better visualized from the quite smaller values of the component v), increasing the discrepancy for smaller values of this amplitude. We can

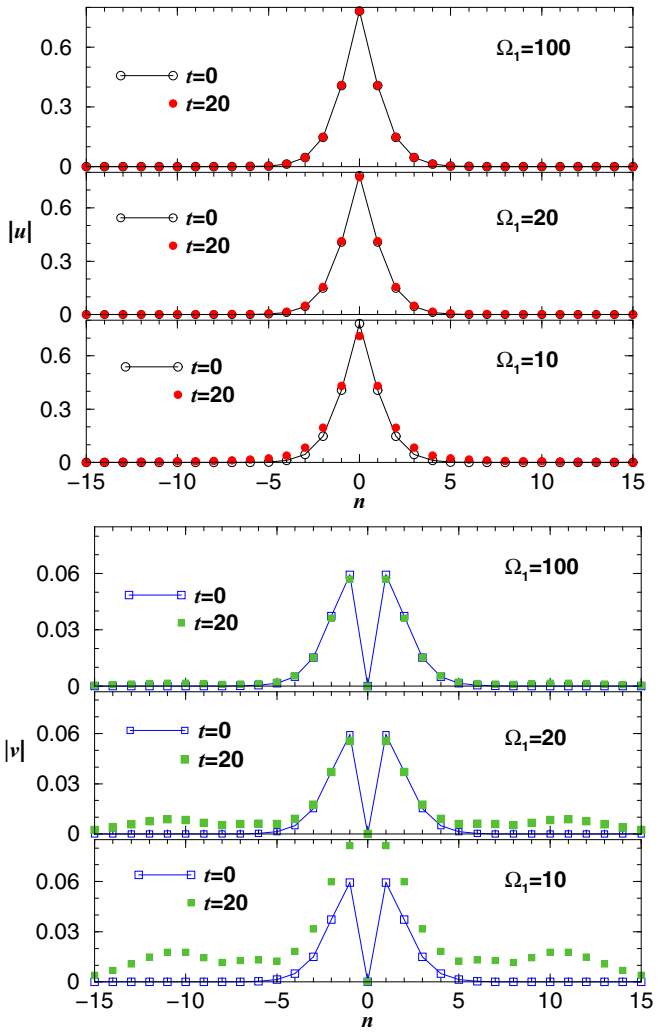

FIG. 8. Full numerical simulations of $|u|$ (upper block of panels) and $|v|$ (lower block of panels) in the ground state, for different amplitude oscillations $\Omega_1 = 10$, 20, and 100 (as shown explicitly), with nonlinearity fixed by $\gamma = -0.8$. The corresponding chemical potential is $\mu = -2.20$, with the other parameters being $\Omega_0 = 1.352$, $\Gamma = 0.3$, $\chi = 1.5$, and $\alpha = 3.83$. In all the simulations, we start relaxation with $\chi_{\rm eff} = \chi J_0(\alpha) = -0.604$ ($t = 0$), performing real-time evolution of Eqs. (8) with $\chi = 1.5$. Plotted quantities are in normalized units.

see from this figure that in the strong modulation limit the eigenmodes of the averaged system are excellent solutions of Eq. (8) for $\Omega_1 = 100$, remaining good even largely below this value (some deviations in the v component start to appear around $\Omega_1 = 20$). From this we conclude that, although from a strict mathematical point of view the averaged theory is valid for $\Omega_1, \omega \to \infty$, the range of applicability of our results is quite large and is likely to be within the present experimental feasibilities.

Besides the stationary ground states considered above, it is also possible to have nonlinear ground-state solutions resembling stripe solutions of the linear system. In this case, stripes are linear superpositions of the degenerated ground states with opposite quasimomentum in the lower branch of the dispersion curve (see Fig. 1). These states can exist

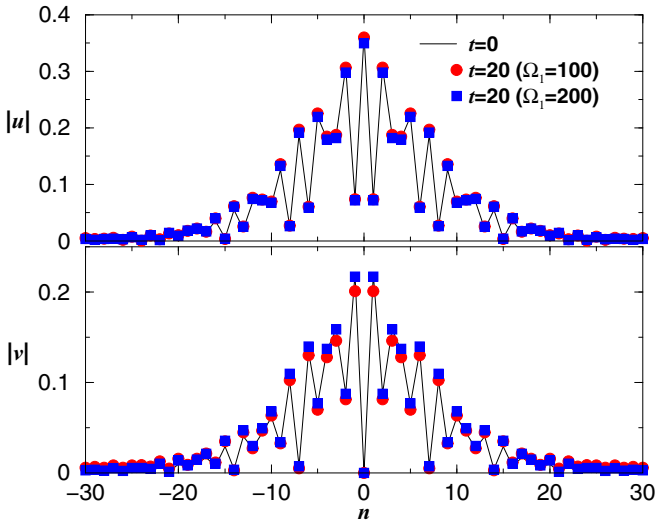

FIG. 9. Ground-state wave-function components, u (upper panel) and v (lower panel), for stripe-soliton solutions from full numerical simulations, for the case with $\chi = 7.5$. The corresponding chemical potential is $\mu = -3.41$. In both the panels, with black-solid lines we have the case with $t = 0$. For $t = 20$, we verify the stability of the results for $\Omega_1 = 100$ (red bullets) and $\Omega_1 = 200$ (blue squares). Except for $\chi = 7.5$, the other parameters are as in Fig. 8. In the simulations, the relaxation is done with $\chi_{\rm eff} = -3.021$, and performance of real-time evolution of Eqs. (8) is done with $\chi = 7.5$. Plotted quantities are in normalized units.

also in the presence of nonlinearity, although not as exact linear combinations, as they have a more complicated format. They can be constructed as long as quasi-double-degenerated minima in the dispersion curve survive in the presence of nonlinearity (this is true for weak nonlinearities). From a numerical point of view, they can be constructed from exact stripes of the linear system, continuing then by a path following method as the nonlinearity is increased.

In Fig. 9, we show results obtained for a stripelike soliton, with $\chi = 7.5$, and for two large values for the amplitude, $\Omega_1 = 100$ and 200 consistent with the ratio, $\alpha = 2\Omega_1/\omega = 3.83$ as in Fig. 8 and at the position $\alpha = \eta_1$. Notice that for the above values the modulated linear dispersion curve has two minima in the lower branch, such that one can directly check the results from the exact modulated dispersion relation, which assures the existence of a linear stripe solution for these parameter values.

From the above results we conclude that the modulation of the Zeeman term can be effectively used for the tuning of the SOC parameter via a simple rescaling in Eq. (18), and, in turn, this permits us to control the energy and the localization properties of the ground-state wave functions.

VI. DISCUSSION AND CONCLUSIONS

Before our concluding remarks, we shall briefly discuss a parameter design for possible experimental observation of the above results. In this respect we refer to the SOC for the case of ^{87}Rb atoms in the field of three laser beams implemented in a tripod scheme. The ground states from the $5S_{1/2}$ manifold are coupled via differently polarized light, by

choosing $|1\rangle = |F = 2, m_F = -1\rangle$, $|2\rangle = |F = 2, m_F = +1\rangle$, and $|3\rangle = |F = 1, m_F = 0\rangle$ [34]. A deep optical lattice can be induced by two additional contrapropagating laser beams of strength of the order ≈ 10 recoil energy. The number of atoms can be taken as $N \approx 3 \times 10^3$, with lattice wavelength $\lambda_L = 1\,\mu$m, radial trapping frequency $\omega_\perp \approx 10^3$ Hz, $a_0 = 100 a_B$ (with a_B, the Bohr radius), and $\omega_R = 2 \times 10^5$ Hz. The strong modulation limit can be reached by considering a modulated Zeeman field of normalized amplitude >20 and frequency of the modulation fixed by $\omega = 2\Omega_1/\alpha$. Under these circumstances, it should be possible to check our results and, in particular, the localized properties of the ground stated at specific values of the modulation parameter discussed above.

In conclusion, we have investigated the effect of a modulating Zeeman field on the energy spectrum and on the eigenstates of a binary BEC mixture in a deep OL and in the presence of SOC, by considering an exact self-consistent numerical diagonalization of the averaged Hamiltonian. Stationary solitonic ground states and stripe modes are also investigated as functions of the modulating parameter, both by exact diagonalizations and by imaginary-time evolution. In particular, we derived proper averaged equations and showed that the chemical potentials of solitonic states display oscillatory behaviors as a function of the tuning parameter α, the amplitudes of which decrease as α is increased. The dependence of the spectrum on the tuning parameter has been fully characterized for the linear SOC system. In this case, the dispersion relations were exactly derived and the extremal curves (ground and highest excited states) of the linear system were shown to be continuous functions, together with their derivatives, consisting of a finite number of band lobes joined by constant lines.

The linear case for BEC with SOC can be experimentally realized, when the interactions are tuned to negligible quantities, by using Feshbach resonance technics, i.e., by the variation of the external magnetic field near the resonant value. As for the nonlinear spectrum, it is shown that the main role of the atomic interactions is to introduce localized states in the band gaps. Remarkably, the structure of the extremal curves of the linear band is well preserved also in the presence of nonlinearity (at least, when such nonlinearities are not too large). The ground-state stability in the presence of a modulating field was demonstrated by real-time evolutions of the original (nonaveraged) system.

Finally, we remark that the control of the localization properties of the ground state of a BEC mixture in a deep optical lattice by means of the SOC parameter could be very useful for applications involving soliton dynamics, including nonlinear Bloch oscillations, dynamical localization, and interferometry. By following the present approach, indeed, one could adjust the Zeeman field so to achieve the maximal localization of a soliton ground state without changing the inter- and intraspecies interactions.

ACKNOWLEDGMENTS

M.S. acknowledges partial support from the Ministero dellIstruzione, dellUniversita e della Ricerca through a Programmi di Ricerca Scientifica di Rilevante Interesse Nazionale initiative under Grant No. 2010HXAW77-005; F.A. acknowledges support from Grant No. FRGS16-013-0512 provided by IIUM(Malaysia) and from a senior visitor fellowship from Conselho Nacional de Desenvolvimento Científico e Tecnológico (CNPq-Brasil). A.G. and L.T. also thank the Brazilian agencies CNPq, Fundação de Amparo à Pesquisa do Estado de São Paulo (FAPESP), and Coordenação de Aperfeiçoamento de Pessoal de Nível Superior (CAPES) for partial support.

[1] R. J. Elliott, Phys. Rev. **96**, 280 (1954).
[2] G. Dresselhaus, A. F. Kip, and C. Kittel, Phys. Rev. **95**, 568 (1954).
[3] G. Dresselhaus, Phys. Rev. **100**, 580 (1955).
[4] E. I. Rashba, Sov. Phys. Solid State **1**, 368 (1959); **2**, 1224 (1960).
[5] Y. A. Bychkov and E. I. Rashba, J. Phys. C **17**, 6039 (1984).
[6] G. Bihlmayer, O. Rader, and R. Winkler, New J. Phys. **17**, 050202 (2015).
[7] M. Z. Hasan and C. L. Kane, Rev. Mod. Phys. **82**, 3045 (2010).
[8] D. Awschalom and N. Samarth, Physics **2**, 50 (2009).
[9] N. Nagaosa, J. Phys. Soc. Jpn. **75**, 042001 (2006); N. Nagaosa, J. Sinova, S. Onoda, A. H. MacDonald, and N. P. Ong, Rev. Mod. Phys. **82**, 1539 (2010).
[10] D. Stepanenko and N. E. Bonesteel, Phys. Rev. Lett. **93**, 140501 (2004).
[11] Y.-J. Lin, K. Jimenez-Garcia, and I. B. Spielman, Nature (London) **471**, 83 (2011).
[12] V. Galitski and I. B. Spielman, Nature (London) **494**, 49 (2013).
[13] Y.-L. Lin, R. K. Compton, K. Jiménez-Garcí a, J. V. Porto, and I. B. Spielman, Nature (London) **462**, 628 (2009).
[14] Q. Zhu, C. Zhang, and B. Wu, Europhys. Lett. **100**, 50003 (2012).
[15] T.-L. Ho and S. Zhang, Phys. Rev. Lett. **107**, 150403 (2011).
[16] Y. Li, L. P. Pitaevskii, and S. Stringari, Phys. Rev. Lett. **108**, 225301 (2012).
[17] M. Levin and A. Stern, Phys. Rev. Lett. **103**, 196803 (2009).
[18] T. A. Sedrakyan, A. Kamenev, and L. I. Glazman, Phys. Rev. A **86**, 063639 (2012).
[19] M. Gong, S. Tewari, and C. Zhang, Phys. Rev. Lett. **107**, 195303 (2011)
[20] C. Zhang, S. Tewari, R. M. Lutchyn, and S. DasSarma, Phys. Rev. Lett. **101**, 160401 (2008)
[21] D. A. Zezyulin, R. Driben, V. V. Konotop, and B. A. Malomed, Phys. Rev. A **88**, 013607 (2013).
[22] M. Merkl, A. Jacob, F. E. Zimmer, P. Ohberg, and L. Santos, Phys. Rev. Lett. **104**, 073603 (2010).
[23] V. Achilleos, D. J. Frantzeskakis, P. G. Kevrekidis, and D. E. Pelinovsky, Phys. Rev. Lett. **110**, 264101 (2013).
[24] L. Salasnich and B. A. Malomed, Phys. Rev. A **87**, 063625 (2013).
[25] Y. Xu, Y. Zhang, and B. Wu, Phys. Rev. A **87**, 013614 (2013).

[26] Y. V. Kartashov, V. V. Konotop, and D. A. Zezyulin, Phys. Rev. A **90**, 063621 (2014).
[27] Y. V. Kartashov, V. V. Konotop, and F. Kh. Abdullaev, Phys. Rev. Lett. **111**, 060402 (2013).
[28] V. E. Lobanov, Y. V. Kartashov, and V. V. Konotop, Phys. Rev. Lett. **112**, 180403 (2014).
[29] Y. Zhang, Y. Xu, and T. Busch, Phys. Rev. A **91**, 043629 (2015).
[30] M. Bukov, Luca D'Alessio, A. Polkovnikov, Adv. Phys. **64**, 139 (2015).
[31] Y. Zhang, G. Chen, and C. Zhang, Sci. Rep. **3**, 1937 (2013).
[32] K. Jiménez-García, L. J. LeBlanc, R. A. Williams, M. C. Beeler, C. Qu, M. Gong, C. Zhang, and I. B. Spielman, Phys. Rev. Lett. **114**, 125301 (2015).
[33] J. Ruseckas, G. Juzeliunas, P. Ohberg, and M. Fleischhauer, Phys. Rev. Lett. **95**, 010404 (2005); G. Juzeliunas, J. Ruseckas, M. Lindberg, L. Santos, and P. Ohberg, Phys. Rev. A **77**, 011802 (2008).
[34] M. J. Edmonds, J. Otterbach, R. G. Unanyan, M. Fleischhauer, M. Titov, and P. Ohberg, New J. Phys. **14**, 073056 (2012).
[35] M. Salerno and F. Kh. Abdullaev, Phys. Lett. A **379**, 2252 (2015).
[36] Y. Zhang, Li Mao, and C. Zhang, Phys. Rev. Lett. **108**, 035302 (2012).
[37] H. Zhai, Int. J. Mod. Phys. B **26**, 1230001 (2012).
[38] P. P. Belicev, G. Gligoric, J. Petrovic, A. Maluckov, L. Hadzievski, and B. A. Malomed, J. Phys. B **48**, 065301 (2015).
[39] M. Salerno, Laser Physics **15**, 620 (2005).
[40] V. V. Konotop and M. Salerno, Phys. Rev. A **65**, 021602(R) (2002).
[41] Y. Suzuki and K. Varga, *Stochastic Variational Approach to Quantum-Mechanical Few-Body Problems*, Lecture Notes in Physics (Springer-Verlag, Heidelberg, 1998).